

EXPERIMENTS AND FAILURE CRITERIA FOR SINGLE CRYSTAL ALLOYS OF GAS TURBINE ENGINE UNDER STATIC AND THERMOCYCLIC LOADING

Getsov L.B.*, Semenov A.S. **, Semenov S.G.** , Tikhomirova E.A.***

* NPO CKTI, ** Saint-Petersburg State Polytechnical University, ***JSK Klimov

Keywords: *single crystal superalloys, creep, plasticity, thermal fatigue, finite element simulation*

Abstract

Results of creep and thermal fatigue experiments on five heat resistant single crystal superalloys with various crystallographic orientations under different temperatures are obtained and discussed with aim to improve models of inelastic deformation and fracture. The dependence of the failure modes (crystallographic or non-crystallographic) on loading regimes is analyzed. The deformation-type criteria of damage accumulation are introduced for the lifetime prediction under static and thermocyclic loading conditions. Experimental results are predicted with acceptable accuracy by using proposed criteria and adequate viscoelastoplastic models of single crystal materials. The proposed criteria of thermal fatigue crack initiation and crack propagation are implemented in the finite element procedure. The results of step-by-step finite element simulations of crack growth under creep and thermal fatigue conditions in the corset specimens are presented and discussed.

1 Introduction

Using of the single crystal superalloys for the manufacturing of gas turbine engine blades allowing a significant increase in the gas temperature before turbine, leads to the necessity to develop more accurate models of inelastic deformation, durability and fracture prediction with aim to improve the reliability of the stress and strength analysis. At the present time there is no any universal justified thermal fatigue criterion and the durability analysis of

the single crystal blades of modern gas turbines requires solving the following problems:

- development and selection of the optimal viscoelastoplastic models, which take into account influence of crystallographic orientation (CGO) on mechanical properties;
- development of the strength criteria, which allow to predict static and thermocyclic crack initiation;
- development of the fracture criterion, which allows to calculate crack growth process in the single crystal under thermocyclic loading.

In the present paper the experimental results and theoretical issues of deformation and fracture models under static and thermocyclic loading are discussed.

2 Materials, research methods and experimental results

The method of thermal fatigue experimental investigation on the corset samples (see Fig. 1) [1, 2] in vacuum condition with and without lateral thermal barrier coatings is widespread in Russia.

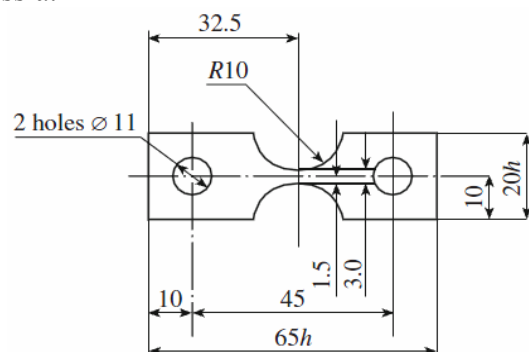


Fig. 1. Corset specimen for thermal fatigue tests.

Thermal fatigue experiments for different temperature regimes, with and without dwells under maximum cycle temperature [2, 3] and creep for five single crystal alloys grades ZhS32, ZhS36, VZhM4, VZhM5U [4] and Alloy 3 with different crystallographic orientation, using for manufacturing of high temperature gas turbine blades are carried out (Fig. 2). The test results are number of cycles to macrocrack initiation and crack rate propagation.

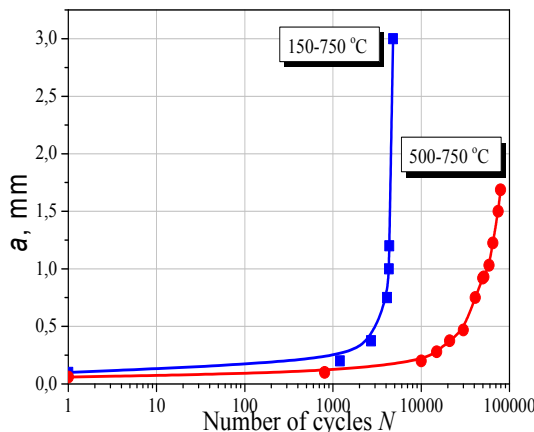


Fig. 2. Curves of thermal fatigue crack growth in the samples [001] from ZHS32 for cycle with $T_{max} = 750 \text{ }^\circ\text{C}$.

Euler angles and Schmid factor are calculated for all specimens. During experiments the formation of the slip bands, initiation and propagation of the microcracks, the macrocrack growth rate were observed using $\times 260$ magnification microscope and logged.

Fractography analysis of the failure cross sections (crack propagation zones), rupture type identification and measurement of irreversible deformation (due to ratcheting) were carried out after experiments. The dependence of fracture modes (crystallographic and noncrystallographic) (Fig. 3 and 4) on test regimes is defined based on obtained experimental results. The dependence of the fracture mode on the crystallographic orientation of specimen is also observed.

Along with thermal fatigue tests on corset samples the creep experiments on cylindrical specimens were carried out with aim to identify material parameters. Fig. 5 shows, as example, the short-term creep curves of the single alloy VZhM5U. Note on the pronounced dominance of III creep stage. The creep curves are obtained

for VZhM4, VZhM5U and Alloy 3 at temperatures from $975 \text{ }^\circ\text{C}$ to $1100 \text{ }^\circ\text{C}$. Results of creep tests for the alloys ZhS32 and ZhS36 are given in [1] and [3].

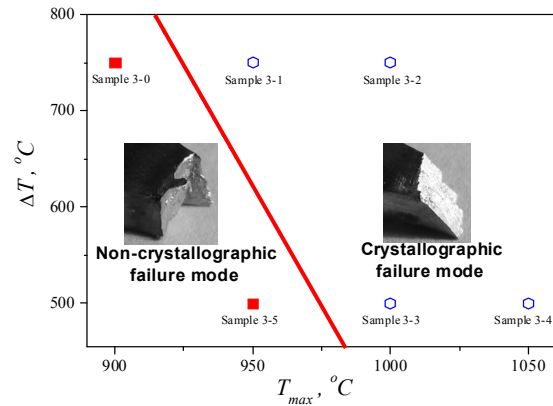


Fig. 3. Map of fracture mechanisms for samples of alloy ZHS36 with the orientations near to [011].

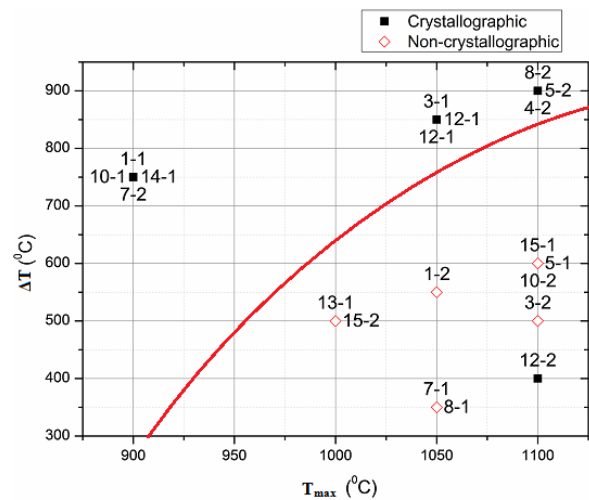


Fig. 4. Map of fracture mechanisms for samples of alloy ZHS32 with orientations near to [001].

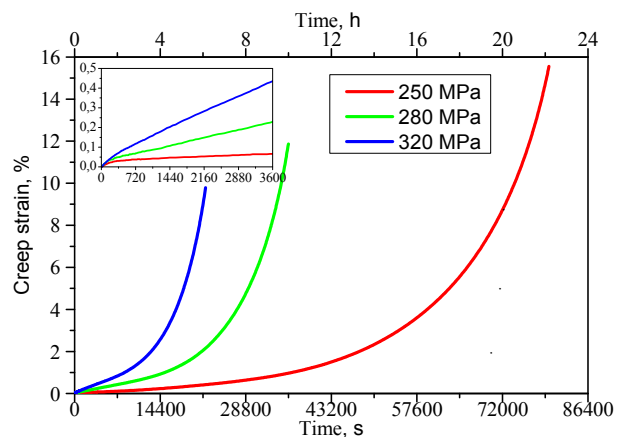


Fig. 5. Creep curves of alloy VZhM5U with crystallographic orientation near to [001] at $1050 \text{ }^\circ\text{C}$.

3 Static loading fracture criteria

The strength of single crystal superalloys under monotonic loading for the complex multiaxial stress state is evaluated by the deformation criteria of Makhutov N.A. [5] or Hancock J.W., Mackenzi A.C. [5,6]:

$$\varepsilon_{eq} - \varepsilon_{r\langle 001 \rangle}^p 1.7 \exp\left(-\frac{1.5\sigma_{mean}}{\sigma_{eq}}\right) = 0, \quad (1)$$

$$\varepsilon_{eq} - \varepsilon_{r\langle 001 \rangle}^p \frac{K_e \sigma_{eq}^2}{3\sigma_1 \sigma_{mean}} = 0, \quad (2)$$

where $\varepsilon_{r\langle 001 \rangle}^p$ is a plastic deformation at rupture, which is determined experimentally under short-term tension in the direction $\langle 001 \rangle$, K_e is a characteristic of the material state (in a brittle state $K_e = 1$, in a viscous state $K_e = 1.2$), $\sigma_{mean} = \frac{1}{3}(\sigma_x + \sigma_y + \sigma_z)$, the equivalent strain measure is defined as follows

$$\varepsilon_{eq} = \sqrt{\frac{2}{9}[(\varepsilon_x - \varepsilon_y)^2 + (\varepsilon_y - \varepsilon_z)^2 + (\varepsilon_z - \varepsilon_x)^2] + \frac{1}{K_f}(\gamma_{xy}^2 + \gamma_{yz}^2 + \gamma_{zx}^2)}, \quad (3)$$

equivalent stress is defined by the expression

$$\sigma_{eq} = \sqrt{\frac{1}{2}[(\sigma_x - \sigma_y)^2 + (\sigma_y - \sigma_z)^2 + (\sigma_z - \sigma_x)^2] + K_f(\tau_{xy}^2 + \tau_{yz}^2 + \tau_{zx}^2)}, \quad (4)$$

where K_f is defined by the plastic deformation at rupture for two orientations

$$K_f = 9 \left[4 \left(\frac{\varepsilon_{r\langle 001 \rangle}^p}{\varepsilon_{r\langle 011 \rangle}^p} \right)^2 - 1 \right]^{-1}. \quad (5)$$

The computation of stress-strain state requires application of inelastic material models accounting plastic and creep effects. The pronounced anisotropy of mechanical properties is exhibit by the elastic and inelastic deformation processes [7]. Neglecting of this fact in some cases leads to the meaningful errors in calculations of stress-strain state. One of the simplest phenomenological plasticity criterion widely used in practice [8-12] for single crystal heat resistant nickel based superalloys is quadratic Hill criterion [13].

Using of the Hill criterion [13, 14]

$$\mathbf{s} \cdot \cdot \mathbf{M} \cdot \cdot \mathbf{s} - 1 = 0, \quad (6)$$

where \mathbf{s} is a deviator of the Cauchy stress tensor $\boldsymbol{\sigma}$, \mathbf{M} is 4th order anisotropy tensor, leads to

the next yield condition formulation for cubic symmetry crystals:

$$\sqrt{\frac{1}{2}[(\sigma_{11} - \sigma_{22})^2 + (\sigma_{22} - \sigma_{33})^2 + (\sigma_{33} - \sigma_{11})^2]} + K_p (\tau_{12}^2 + \tau_{23}^2 + \tau_{31}^2) = \sigma_T \quad (7)$$

There are two arbitrary stress states experiments is enough to defining of the yield criterion constants σ_T and K_p . For isotropic body $K_p = 3$ and instead of (6) we got the von Mises criteria. The dependences of K_p on temperature for single crystal alloys are showed in Fig. 6.

The coefficient K_p is defined by the yield stresses for two orientations as follows

$$K_p = 4 \left(\frac{\sigma_{T\langle 001 \rangle}}{\sigma_{T\langle 011 \rangle}} \right)^2 - 1 \quad (8a)$$

or alternatively by the expression

$$K_p = 3 \left(\frac{\sigma_{T\langle 100 \rangle}}{\sigma_{T\langle 111 \rangle}} \right)^2. \quad (8b)$$

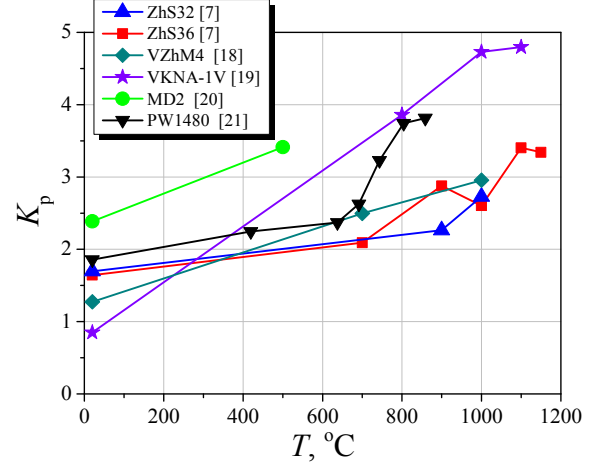


Fig. 6. Temperature dependence of K_p .

Shmid criterion [15, 14]

$$\min_{\alpha} \frac{1}{\tau_0} \mathbf{P}^{\alpha} \cdot \cdot \boldsymbol{\sigma} - 1 = 0, \quad (9)$$

where $\mathbf{P}^{\alpha} = \frac{1}{2}(\mathbf{n}^{\alpha} \mathbf{1}^{\alpha} + \mathbf{1}^{\alpha} \mathbf{n}^{\alpha})$ denotes a Shmid tensor, is used as plasticity criterion in the micromechanical models [16, 17 etc.], which take into account that the deformation process is a result of slipping in active crystallographic slip systems.

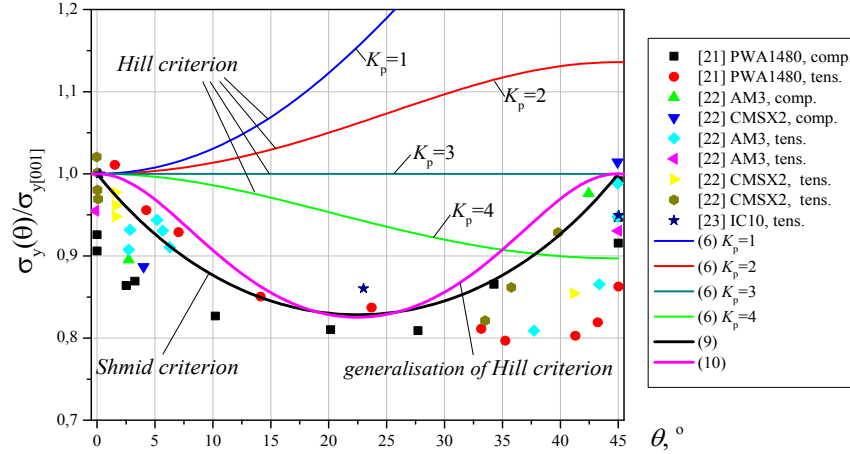


Fig. 7. Comparison of yield stresses for Shmid and Hill criteria with experimental data ([21-23]) for uniaxial tension under different loading orientation to the crystallographic direction $[001]$ in the plain (100) .

The performed investigations are shown the advantage of Shmid micromechanical model than Hill phenomenological model (see Fig. 7).

The more complex phenomenological plasticity criterion proposed in [14]

$$\mathbf{s}^2 \cdot \cdot \mathbf{N} \cdot \cdot \mathbf{s}^2 - (\mathbf{s} \cdot \cdot \mathbf{M} \cdot \cdot \mathbf{s})^2 - 1 = 0 \quad (10)$$

as Hill criterion generalization with aim to improve prediction accuracy.

4 Thermal fatigue damage criteria

The prediction of TMF failure of single crystal materials is performed on the basis of the deformation criterion [24-26]. The macrocrack initiation criterion is a condition for achieving critical value of the total damage initiated by different mechanisms:

$$D_1(\Delta \varepsilon_{eq}^p) + D_2(\Delta \varepsilon_{eq}^c) + D_3(\varepsilon_{eq}^p) + D_4(\varepsilon_{eq}^c) = 1 \quad (11)$$

The criterion (11) is based on a linear damage summation of: cyclic plastic strain

$$D_1 = \sum_{i=1}^n \frac{(\Delta \varepsilon_{eq_i}^p)^k}{C_1(T_i)}, \quad (12)$$

cyclic creep strain

$$D_2 = \sum_{i=1}^n \frac{(\Delta \varepsilon_{eq_i}^c)^m}{C_2(T_i)}, \quad (13)$$

one-sided accumulated plastic strain

$$D_3 = \max_{0 \leq t \leq t_{\max}} \frac{\varepsilon_{eq}^p}{\varepsilon_r^p(T)} \quad (14)$$

and one-sided accumulated creep strain

$$D_4 = \max_{0 \leq t \leq t_{\max}} \frac{\varepsilon_{eq}^c}{\varepsilon_r^c(T)}, \quad (15)$$

where C_1 , C_2 , k , m , ε_r^p , ε_r^c are material parameters, depending on the temperature and a crystallographic orientation. Usually the relations $k=2$, $m=5/4$, $C_1 = (\varepsilon_r^p)^k$, $C_2 = (\frac{3}{4}\varepsilon_r^c)^m$ are used [24].

The different norms of strain tensor are considered as equivalent strain in the criteria (11) for single crystal alloys, among them there are: the *maximum shear strain in slip system* with normal $\mathbf{n}_{\{111\}}$ to slip plane and slip direction $\mathbf{l}_{\langle 011 \rangle}$

$$\varepsilon_{eq} = \mathbf{n}_{\{111\}} \cdot \boldsymbol{\varepsilon} \cdot \mathbf{l}_{\langle 011 \rangle}, \quad (16)$$

the *maximum principal strain* (maximum eigenvalue of the strain tensor)

$$\varepsilon_{eq} = \varepsilon_1 = \max \arg \{ \det(\boldsymbol{\varepsilon} - \lambda \mathbf{1}) = 0 \}, \quad (17)$$

the *strain intensity von Mises*

$$\varepsilon_{eq} = \sqrt{\frac{2}{9} [(\varepsilon_x - \varepsilon_y)^2 + (\varepsilon_y - \varepsilon_z)^2 + (\varepsilon_z - \varepsilon_x)^2] + \frac{1}{3} (\gamma_{xy}^2 + \gamma_{yz}^2 + \gamma_{zx}^2)}, \quad (18)$$

the *strain intensity of Hill*

$$\varepsilon_{eq} = \sqrt{\frac{2}{9} [(\varepsilon_x - \varepsilon_y)^2 + (\varepsilon_y - \varepsilon_z)^2 + (\varepsilon_z - \varepsilon_x)^2] + \frac{1}{K_f} (\gamma_{xy}^2 + \gamma_{yz}^2 + \gamma_{zx}^2)} \quad (19)$$

and the *maximum shear strain*

$$\varepsilon_{eq} = \frac{1}{2} [\varepsilon_1 - \varepsilon_3]. \quad (20)$$

The equivalent strains (16) and (19) correspond to the crystallographic failure mode, while equivalent strains (17), (18) and (20) correspond to the non-crystallographic failure mode. In (19) K_f is defined by (5).

5 Finite element computation of the stress-strain state of single crystal corset specimens

In order to verify the thermal fatigue criterion (11) the nonlinear stress-strain analysis of single crystal corset samples (see Fig. 1) was carried out using the finite-element (FE) program PANTOCRATOR [27] with an application of micromechanical models of elastoplasticity and viscoelastoplasticity. These material models take into account that the inelastic deformation occurs in accordance with crystal slip systems by a slip mechanism and therefore deformation is strongly sensitive to the crystallographic orientation. The elastoplastic and viscoelasto-plastic material models [16, 17] with nonlinear kinematic and isotropic hardening also accounting the selfhardening on each system and the latent hardening [28] between slip systems are used in FE simulations. The application of viscoelastic models leads to unrealistically overestimated levels of stress.

The obtained results for inhomogeneous stress, strain and damage fields allow to find the location of crack initiation. The damage field is obtained by the criterion (11) on the basis of analysis of strain field evolution using the experimental data on creep and elastoplastic deformation curves. The typical damage field distribution after 10th thermal cycle (20°C → $T_{max}=900^{\circ}C \leftrightarrow T_{min}=150^{\circ}C$) is presented in Fig. 8 for the sample from alloy VZhM4 with the orientation near to $\langle 001 \rangle$. The best prediction (in a comparison with experiment) of the number of cycles for the crack initiation is given by the strain measure (16) in this loading case.

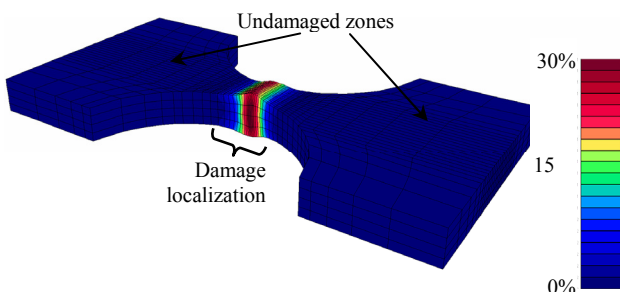


Fig. 8. Damage field distribution after 10th cycle for the sample 43 from alloy VZhM4 with the crystallographic orientation near to $\langle 001 \rangle$.

The results of the FE simulations show that the crystallographic orientation has a significant influence on the stress-strain state of the samples (see Fig. 9), as also confirmed by the experiments [2, 26].

The results of verification of criterion (11) for alloy ZhS36 are given in Fig. 10. The computed number of cycles of crack initiation demonstrates satisfactory accuracy.

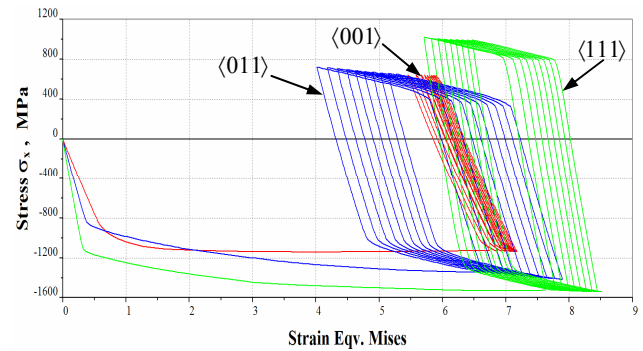


Fig. 9. Influence of crystal orientation on cyclic stress-strain curve. Results of finite-element simulations for thermal cycles with $T_{min}=150^{\circ}C$ and $T_{max}=900^{\circ}C$ (central point of specimen).

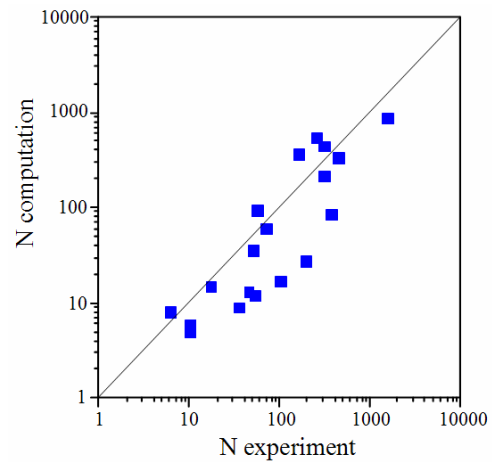


Fig. 10. Comparison of the number of cycles until a macrocrack initiation in the samples of alloy ZHS36 using deformation criterion (11) and the experimental results.

6 Thermal fatigue crack propagation

The direction of the crack propagation in a single crystal is defined by the *crystallographic* structure (typically it is a plane $\langle 111 \rangle$ for considered alloys [29, 30]) at crystallographic mode of failure and correspondingly the direction is defined by the stress state at *non-crystallographic* failure mode (high temperature).

The criterion of thermal-fatigue crack propagation [31, 32], which is based on linear summation of the contributions from the fatigue and creep, is used in order to determine the rate of crack propagation and number of cycles to failure. The criterion is based on using stress intensity factor ΔK_{eff} (for the description of the fatigue) and C^* -integral (for the description of the creep during the holding time at the maximum temperature of the cycle). A mathematical formulation of the criterion represents a generalization of Paris power type equation by taking into account two mechanisms of cracking [31]:

$$\frac{da}{dN} = B(\Delta K_{eff})^m + \int_0^{t_{cyc}} A(C^*(\tau))^q d\tau, \quad (21)$$

where A, B, m, q are material constants, which are defined separately from fatigue experiments as $\frac{da}{dN}(\Delta K_{eff})$ and creep experiments as $\frac{da}{dt}(C^*)$ crack growth data.

The crack propagation process in the corset sample (see Fig. 1) from alloy ZhS36 is direct cycle by cycle simulated using FE program ABAQUS [33]. The specimen has CGO near $\langle 001 \rangle$. The deviation from the axial orientation is 5.47° , from azimuthal is 41.97° (Euler's angles for rotations ZX'Z': $\varphi=354.7^\circ$, $\theta=41.7^\circ$, $\psi=89.8^\circ$). The CGO was determined by Laue's diffraction patterns.

The location of crack initiation is defined by FE damage analysis (see section 5) and it also corresponds to the experimentally observed. The crack propagates in the plane $\langle 111 \rangle$ (see Fig. 11) except the rupture stage. The crack propagation process is simulated only in the plane $\langle 111 \rangle$ without out-plane deviations by means step-by-step technique with FE remeshing at environment of a crack front at the every step. The initial crack front is taken elliptic form. ΔJ_{eff} integral is used to calculate ΔK_{eff} . Fracture zone is established by comparison calculated J integral with J_{Ic} value. The details of simulation are described in [31, 32].

In the experiment the sample failed after 560 thermal cycles ($T_{min}=150^\circ C \leftrightarrow T_{max}=900^\circ C$), in which the registered crack initiation stage lasted 435 cycles and crack propagation stage was 125

cycles. The comparison of the computed number of cycles for crack propagation stage with experimental results is given in Table 1. The results of FE simulations of the crack growth in single crystal corset specimen are presented in Fig. 12. Note on the extended plastic zones in the crack growth area.

The simulated crack front evolution is shown in Fig. 13a. It demonstrates a good correlation with data of fractography analysis (Fig. 13b).

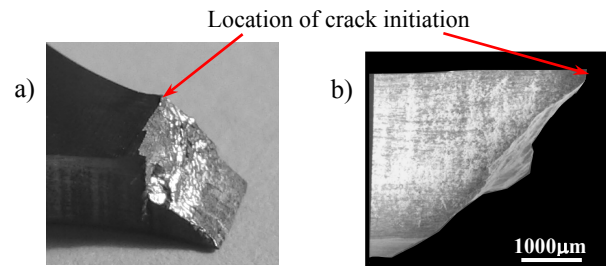


Fig. 11. Specimen from alloy ZhS36 after failure: a) left half, b) right half.

Table 1. Comparison of the estimated number of cycles for crack propagation stage with experimental results (alloy ZhS36).

	Number of cycles
FE computation	192
Experiment	125

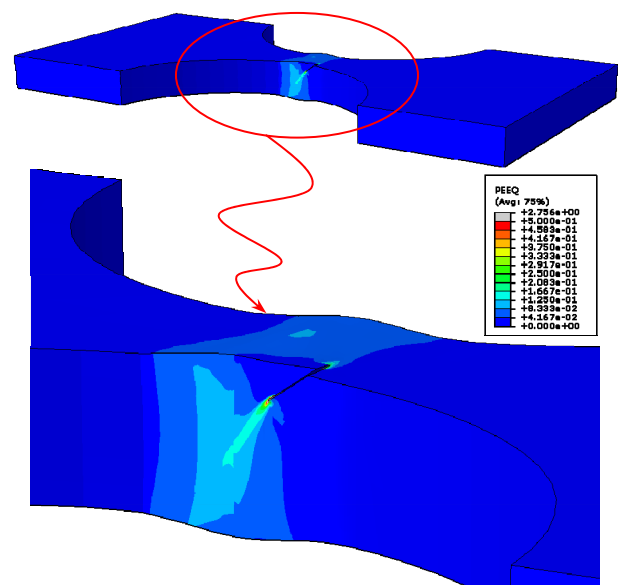


Fig. 12. Plastic strain intensity field distribution in the specimen from alloy ZhS36 with crack of length 0.5 mm.

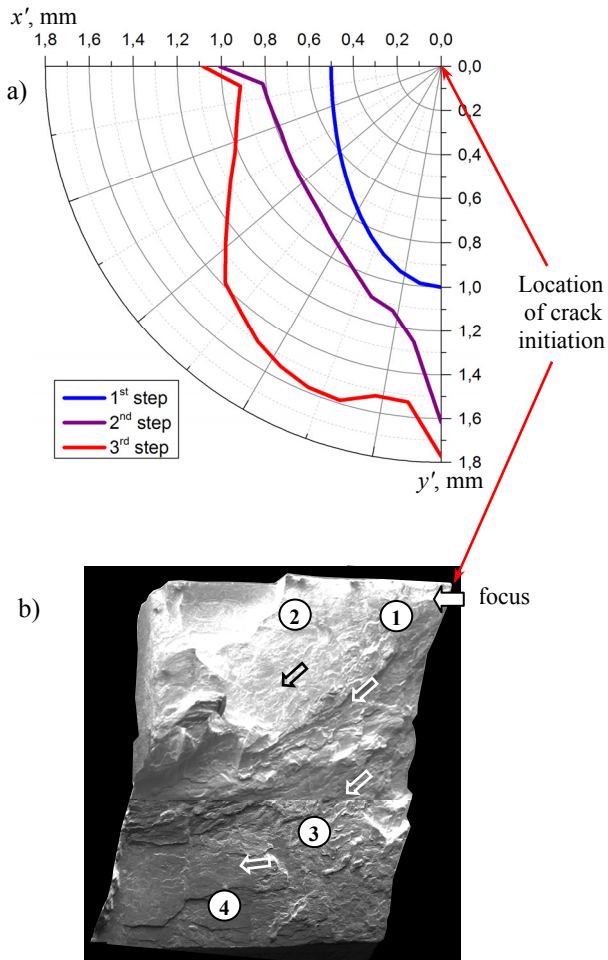


Fig. 13. Evolution of the thermal fatigue crack front propagation on the fracture surface: a) results of finite element simulations, b) data of the fractography analysis (specimen from alloy ZhS36).

7 Conclusions

1. Thermal fatigue tests were performed on corset samples from five different single crystal nickel-based superalloys with various crystallographic orientations under different temperatures and cycle durations with aims to determine the characteristics of the thermal fatigue resistance and to formulate thermal fatigue failure criterion.
2. The crack initiation criterion for the single crystal alloys under thermal cyclic loadings is proposed and discussed. The satisfactory correlation is observed between the proposed deformation criterion (11) and obtained experimental results.
3. The finite element simulations of single crystal corset specimens under thermal cyclic loading have been performed by using different material models. The obtained results indicate an applicability of the proposed deformation criteria of failure for the five considered single crystal alloys for the temperatures up to 1100°C.

4. The high sensitivity of the thermal fatigue durability to the crystallographic orientation and to the thermal cycle parameters is observed experimentally and also in the corresponding finite-element simulations on corset specimens.
5. The proposed crack propagation criterion (21) under thermal cyclic loadings demonstrates satisfactory accuracy in comparison with the experimental number of cycles to failure and the crack front evolution by data of the fractography analysis.
6. The reliable analysis of thermal fatigue strength and durability of single crystal blades of GTE requires further detailed studies the materials characteristics in wide range of temperatures, including the crack resistance parameters.

References

- [1] Getsov LB, Semenov AS, Tikhomirova EA and Rybnikov AI. Failure criteria for single crystal alloys of gas turbine blades under static and thermocyclic loading. *Proc. of 19th European Conference on Fracture. Fracture Mechanics for Durability, Reliability and Safety*, Kazan, pp 670-678, 2012.
- [2] Getsov LB, Dobina NI, Rybnikov AI, Semenov AS, Staroselskii A and Tumanov NV. Thermal fatigue resistance of a monocrystalline alloy. *Strength of materials*, Vol. 40, No. 5, pp 538-551, 2008.
- [3] Getsov LB. *Materials and strength of gas turbine parts*. Vol. 1 and 2, Publ. House. Gas Turbine Technology, 2011.
- [4] Toloraya VN, Orekhov NG and Chubarova EN. Carbon-free Re-containing nickel alloy for turbine blades. *Liteinoye proizvodstvo*, No. 6, pp 25-30, 2012.
- [5] Getsov LB, Margolin BZ and Fedorchenko DG. The determination of elements of engineering safety margins in the calculation of structures by finite element method. *Proc. NPO CKTI, Strength of materials and resource elements of power*. No. 296, pp 51-66, 2009.
- [6] Hancock JW and Mackenzi AC. On the mechanisms of ductile failure in high strength steel subjected to multi-axial stress state. *J. Mech. Phys. Solids*. Vol. 24, No. 213, pp 147-149, 1976.
- [7] Shalin RE, Svetlov IL, Kachanov EB, Toloraiya VN and Gavrilin OS. *Single crystals of nickel-base superalloys*. Mechanical Engineering, 1997.
- [8] Nouailhas D and Freed AD. A viscoplastic theory for anisotropic materials. *J. Eng. Mater. Technol*, Vol. 114, No. 1, pp 97-104, 1992.
- [9] Choi SH and Krempl E. Viscoplasticity theory based on overstress applied to the modeling of cubic single crystals. *European J. of Mechanics-A. Solids*, Vol. 8, No. 2, pp 219-233, 1989.
- [10] Magerramova LA and Vasil'ev BE. Choosing of anisotropy model of single crystal alloy for strength

- computations of gas turbine engine blades using modern software. Proc. of TSIAM, No. 1344, pp 341-350, 2010.
- [11] Magerramova LA and Vasil'ev BE. Azimuth orientation influence on the stress-strain state and strength of high-temperature gas turbines single crystal blades. Bulletin UGATU, Vol. 15, No. 4(44), pp 54-58, 2011.
- [12] Getsov LB, Mikhailov VE, Semenov AS, Krivonosova VV, Nozhnitsky YuA, Blinnik BS and Magerramova LA. Computational determination of GTE blades and vanes life. Part 2. Single crystal alloys. *Gas turbo technology*, No. 8, pp 18-25, 2011.
- [13] Hill R. A theory of the yielding and plastic flow of anisotropic metals. *Proc R Soc London*, Vol. 1033, No. 193, pp 281-297, 1948.
- [14] Semenov AS. The identification of anisotropy parameters of phenomenological plasticity criterion for single crystals worked out on the micro-mechanical model basis. *St. Petersburg State Polytechnical University Journal. Physics and Mathematics*, Vol. 194, Iss. 2, pp 17-29, 2014.
- [15] Schmid E and Boas W. *Kristallplastizität mit besonderer Berücksichtigung der Metalle*. Springer, 1935.
- [16] Cailletaud G. A micromechanical Approach to Inelastic Behaviour of Metals. *International Journal of Plasticity*, 1991, Vol. 8, pp 55-73.
- [17] Besson J, Cailletaud G, Chaboche JL, Forest L. *Non-Linear Mechanics of Materials*. Publ. of St. Petersburg State Polytechnical University, 2010.
- [18] Kablov EN, Petrushin NV, Svetlov IL and Demonis IM. New generation of casting nickel heat-resistant alloys. *Proc. VIAM*, pp 36-52, 2012.
- [19] Bulygin IP, Buntushkin VP and Bazyleva OA. Casting alloy based on intermetallid Ni₃Al for single crystal turbine blades. *Aviation industry*, No. 3-4, pp 61-65, 1997.
- [20] Segersäll M. *Nickel-based single-crystal superalloys - the crystal orientation influence on high temperature properties*. PhD Thesis. Linköping University, 2013.
- [21] Shah DM and Duhl DN The effect of orientation, temperature and grain size on the yield strength of a single crystal nickel base superalloy. *Superalloys. The Metallurgical Society of AIME*, pp 105-114, 1984.
- [22] Hoinard G, Estevez R and Franciosi P. Hardening anisotropy of γ/γ' superalloy single crystals. 1. Experimental estimates at 650 °C from a homogeneous analysis. *Acta Metall. Mater*, Vol. 43, pp 1593-1607, 1995.
- [23] Lei C, Weidong W, Haitao C, Hongjian Z and Ying X. Yield anisotropy and tension/compression asymmetry of a Ni₃Al based intermetallic alloy. *Chinese Journal of Aeronautics*, Vol. 26(3), pp 801-806, 2013.
- [24] Semenov AS and Getsov LB. Thermal fatigue fracture criteria of single crystal heat-resistant alloys and methods for identification of their parameters. *Strength of Materials*, Vol. 46, No. 1, p 38-48, 2014.
- [25] Getsov LB, Semenov AS, Tikhomirova EA and Rybnikov AI. Thermocyclic- and static-failure criteria for single-crystal superalloys of gas-turbine blades. *Materials and Technology*, Vol. 48, No 2, pp 255-260, 2014.
- [26] Getsov L, Semenov A and Staroselsky A. A failure criterion for single crystal superalloys during thermocyclic loading. *Materials and Technology*. Vol. 42, pp 3-12, 2008.
- [27] Semenov AS. PANTOCRATOR-finite-element software package, focused on the solution of nonlinear problems in mechanics. *Proc. of V Int. Conf. "Scientific and technical problems of forecasting the reliability and durability of the structures and methods for their solution"*, St. Petersburg, pp 466-480, 2003.
- [28] Kocks UF and Brown TJ. Latent hardening in aluminium. *Acta Metall*. Vol. 14, pp 87-98, 1966.
- [29] Reed PAS, Wu XD and Sinclair I. Fatigue crack path prediction in UDIMET 720 nickel-based alloy single crystals *Met. and Mater. Transact*. Vol. 31A, pp 109-123, 2000.
- [30] Telesman J and Ghosn LJ. Accelerated fatigue crack growth behavior of PWA1480 single crystal alloy and its dependence on the deformation mode. *Superalloys '88*, pp 615-624, 1988.
- [31] Semenov AS, Semenov SG, Nazarenko AA, Getsov LB. Computer simulation of fatigue, creep and thermal-fatigue cracks propagation in gas-turbine blades. *Materials and Technology*, Vol. 46, No 3, pp 197-203, 2012.
- [32] Semenov AS, Semenov SG, Nazarenko AA, Getsov LB. Computational-experimental method of fatigue, creep and thermal fatigue crack growth kinetics in the GTE blades. *Russian Journal of Heavy Machinery*, No. 11-12, pp 7-20, 2013.
- [33] ABAQUS Analysis User's Manual, Version 6.10.

Contact Author Email Address

semenov.artem@googlemail.com

Copyright Statement

The authors confirm that they, and/or their company or organization, hold copyright on all of the original material included in this paper. The authors also confirm that they have obtained permission, from the copyright holder of any third party material included in this paper, to publish it as part of their paper. The authors confirm that they give permission, or have obtained permission from the copyright holder of this paper, for the publication and distribution of this paper as part of the ICAS 2014 proceedings or as individual off-prints from the proceedings.